Targeting Somatostatin Receptors: Preclinical Evaluation of Novel ^{18}F-Fluoroethyltriazole-Tyr^3-Octreotate Analogs for PET

Julius Leyton[1], Lisa Iddon[2], Meg Perumal[1], Bard Indrevoll[3], Matthias Glaser[2], Edward Robins[2], Andrew J.T. George[4], Alan Cuthbertson[3], Sajinder K. Luthra[2], and Eric O. Aboagye[1]

[1]Comprehensive Cancer Imaging Center at Imperial College, Faculty of Medicine, Imperial College London, London, United Kingdom; [2]MDx Discovery (part of GE Healthcare) at Hammersmith Imanet Ltd., Hammersmith Hospital, London, United Kingdom; [3]GE Healthcare AS, Oslo, Norway; and [4]Section of Immunobiology, Faculty of Medicine, Imperial College London, London, United Kingdom

The incidence and prevalence of gastroenteropancreatic neuroendocrine tumors has been increasing over the past 3 decades. Because of high densities of somatostatin receptors (sstr)—mainly sstr-2—on the cell surface of these tumors, ^{111}In-diethylenetriaminepentaacetic acid-octreotide scintigraphy has become an important part of clinical management. ^{18}F-radiolabeled analogs with suitable pharmacokinetics would permit PET with more rapid clinical protocols. **Methods:** We compared the affinity in vitro and tissue pharmacokinetics by PET of 5 structurally related ^{19}F/^{18}F-fluoroethyltriazole-Tyr^3-octreotate (FET-TOCA) analogs: FET-G-polyethylene glycol (PEG)-TOCA, FETE-PEG-TOCA, FET-G-TOCA, FETE-TOCA, and FET-βAG-TOCA to the recently described ^{18}F-aluminum fluoride NOTA-octreotide (^{18}F-AlF-NOTA-OC) and the clinical radiotracer ^{68}Ga-DOTATATE. **Results:** All ^{19}F-fluoroethyltriazole-Tyr^3-octreotate compounds retained high agonist binding affinity to sstr-2 in vitro (half-maximal effective concentration, 4–19 nM vs. somatostatin at 5.6 nM). Dynamic PET showed that incorporation of PEG linkers, exemplified by ^{18}F-FET-G-PEG-TOCA and ^{18}F-FETE-PEG-TOCA, reduced uptake in high sstr-2–expressing AR42J pancreatic cancer xenografts. ^{18}F-FET-βAG-TOCA showed the lowest nonspecific uptake in the liver. Tumor uptake increased in the order ^{68}Ga-DOTATATE $<$ ^{18}F-AlF-NOTA $\leq$ ^{18}F-FET-βAG-TOCA $<$ ^{18}F-FET-G-TOCA. The uptake of ^{18}F-FET-βAG-TOCA was specific: a radiolabeled scrambled peptide, ^{18}F-FET-βAG-[W-c-(CTFTYC)K], did not show tumor uptake; there was lower uptake of ^{18}F-FET-βAG-TOCA in AR42J xenografts when mice were pretreated with 10 mg of unlabeled octreotide per kilogram; and there was low uptake of ^{18}F-FET-βAG-TOCA in low sstr-2–expressing HCT116 xenografts. **Conclusion:** We have developed novel fluoroethyltriazole-Tyr^3-octreotate radioligands that combine high specific binding with rapid target localization and rapid pharmacokinetics for high-contrast PET. ^{18}F-FET-βAG-TOCA and ^{18}F-FET-G-TOCA are candidates for future clinical evaluation.

Received Feb. 3, 2011; revision accepted May 10, 2011.

For correspondence or reprints contact: Eric O. Aboagye, Molecular Therapy Group, Faculty of Medicine, Imperial College London, Room 240 MRC Cyclotron Building, Hammersmith Hospital, Du Cane Rd., London, W12 ONN, United Kingdom

E-mail: eric.aboagye@imperial.ac.uk

Published online Aug. 18, 2011.

Key Words: somatostatin receptor; octreotide; ^{18}F-fluoroethyltriazole-Tyr^3-octreotate; positron emission tomography; and neuroendocrine

J Nucl Med 2011; 52:1441–1448
DOI: 10.2967/jnumed.111.088906

The incidence and prevalence of gastroenteropancreatic neuroendocrine tumors (GEP-NETs) has increased significantly over the past 3 decades (*1*). The most common site of primary GEP-NETs is the gastrointestinal tract (60%). Within the gastrointestinal tract, the single most common site is the small intestine (34%), followed by the rectum (23%), colon (19%), stomach (8%), pancreas (8%), and appendix (7%). There is no standard management of GEP-NETs, although the recent PROMID trial suggested a response benefit in the use of sandostatin LAR Depot (octreotide acetate for injection suspension; Novartis Pharmaceuticals) in patients with metastatic midgut tumors (*2*). Targeted therapies, including everolimus and sunitinib, are being investigated (*3*). Treatment of pancreatic neuroendocrine patients with everolimus, for example, has shown prolongation of progression-free survival (*4*). Other treatment options include radiolabeled somatostatin analogs and surgical debulking; however, no improvements in survival have been reported, and validated biomarkers for response are lacking.

Currently somatostatin-receptor (sstr) imaging is the method of choice for the staging of GEP-NETs. Somatostatin [H-Ala^1-Gly^2-c(Cys^3-Lys^4-Asn^5-Phe^6-Phe^7-Trp^8-Lys^9-Thr^{10}-Phe^{11}-Thr^{12}-Ser^{13}-Cys^{14})-OH] is a small regulatory peptide that has an inhibitory effect on the production of several exocrine hormones (prolactin, insulin, glucagon, and thyroid-stimulating hormone) in the gastrointestinal tract and antiproliferative effects. sstrs are G-protein–coupled receptors expressed on cell membranes, which on ligand binding generate a transmembrane signal. Five receptor subtypes (sstr-1–sstr-5) have been identified to date

(*5*). GEP-NETs frequently express a high density of sstr, in particular sstr-2, that can be exploited for imaging, from identifying a small primary lesion after biochemical syndrome diagnosis and selecting patients for radiotherapy to exploring the extent of metastatic disease (*6–8*). Somatostatin analogs have been developed because somatostatin itself has a short plasma half-life (~3 min). The current somatostatin receptor–based clinical standard for functional imaging of GEP-NETs is scintigraphy with ^{111}In-diethylenetriaminepentaacetic acid (DTPA)-octreotide (half-life of ^{111}In, 2.8 d; photon energy, 254 keV) (*9*); clinical imaging is then performed at 1–2 d after injection of the radiopharmaceutical to ensure sufficient target-to-background contrast. Octreotide [(D)-Phe^1-c(Cys^2-Phe^3-(D)-Trp^4-Lys^5-Thr^6-Cys^7)Thr-ol^8] binds with high affinity to sstr-2 and to a lesser extent sstr-5 (*10*). Substitution of Phe^3 by Tyr^3, as well as C-terminal Thr(ol)^8 by Thr^8, gives Tyr^3-octreotate [(D)-Phe^1-c(Cys^2-Tyr^3-(D)-Trp^4-Lys^5-Thr^6-Cys^7)Thr^8], with improved selectivity and affinity for sstr-2, compared with octreotide (*8,11,12*).

PET offers better image contrast than scintigraphy, and indeed octreotide analogs using radiometals such as ^{68}Ga (1.1-h half-life, 90% β^+, 1.9-MeV $E_{\beta+}$ [positron energy]) and ^{64}Cu (12.7-h half-life, 19% β^+, 0.6-MeV $E_{\beta+}$; also emission of 30% β^- particles) have been developed for peptide-based imaging by PET (*13–15*). A good correlation between the uptake of ^{68}Ga-labeled peptides and sstr-2 immunohistochemistry has been demonstrated in patients, supporting the use of these radioligands for imaging of sstr-2 (*16*). Peptides labeled with the ^{18}F radioisotope, having the optimal combination of half-life, photon flux, and photon energy (1.8-h half-life, 97% β^+, 0.6-MeV $E_{\beta+}$), should be superior to the metal-based tracers and be devoid of nonspecific uptake resulting from transchelation (*17*). Consequently, ^{18}F-labeled octreotide analogs have previously been developed (*18–20*). Tyr^3-octreotate has been radiolabeled with both ^{68}Ga and ^{18}F radioisotopes for PET of tumors (*21,22*). In this article, we explored the relatively new copper-catalyzed azide-alkyne cycloaddition reaction (click reaction) to design several octreotate analogs. Marik and Sutcliffe (*23*), and Glaser and Årstad (*24*) were the first to apply click chemistry to ^{18}F radiolabeling of various building blocks or peptides. Since then, the click reaction has been used for rapid chemoselective and regiospecific ^{18}F radiolabeling of peptides under mild reaction condition, with good synthetic yields (*25,26*). The Tyr^3-octreotate core was selected over octreotide because of its superior sstr-2 specificity, higher affinity, and tumor uptake properties (*8,12*). Rapid tumor accumulation, together with rapid clearance of labeled peptides from normal tissues including the liver and muscle, is a prerequisite for use of short-lived positron-emitting radioisotopes such as ^{18}F. Recognizing that incorporation of polyethylene glycol (PEG) moiety and length or type of linker used to connect the peptide core to the ^{18}F-containing prosthetic group can change peptide disposition, we performed a comparative study to evaluate tissue pharmacokinetics and imaging properties of 5 structurally related ^{18}F-fluoroethyltriazole-Tyr^3-octreotate (FET-TOCA) analogs—FET-G-PEG-TOCA, FETE-PEG-TOCA, FET-G-TOCA, FETE-TOCA, and FET-βAG-TOCA (Fig. 1)—and compared these to a scrambled labeled peptide, the recently described ^{18}F-aluminum fluoride NOTA-octreotide (^{18}F-AlF-NOTA-OC (*19*)) and the clinically used radiotracer ^{68}Ga-DOTATATE. Assessment of the pharmacokinetics and imaging properties in vivo should provide structure–activity relationship data for selection of the optimal radiotracer.

MATERIALS AND METHODS

Radiochemicals and Log D Measurements

Five structurally related ^{19}F/^{18}F fluoroethyltriazole-Tyr^3-octreotate analogs (Supplemental Fig. 1; supplemental materials are available online only at http://jnm.snmjournals.org) and a related scrambled peptide were prepared. All commercially available chemicals were of analytic grade and used without further purification. Stable ^{19}F was used for assays in which radioactivity was not needed. The synthesis of the radiotracers by click radiochemistry (Supplemental Fig. 1) is reported in detail elsewhere (*27*). Labeled products were eluted with ethanol in 100-μL fractions and made up to a 10% ethanol/phosphate-buffered saline solution (pH 7.4). ^{18}F-AlF-NOTA was synthesized as previously described (*19*). ^{68}Ga-DOTATATE was purchased from Covidien (U.K.) Commercial Ltd. The lipophilicity (Log D) of the radiotracers has been reported (*27*).

In Vitro Binding Assay

Tyr^3-octreotate analogs bind mainly to sstr-2. The affinity of stable ^{19}F-fluoroethyltriazole-Tyr^3-octreotate analogs for somatostatin receptor subtype sstr-2, versus sstr-4 as control low-affinity-receptor subtype, was determined using a fluorometric imaging plate reader assay. The assay involved measuring the ^{19}F-fluoro-

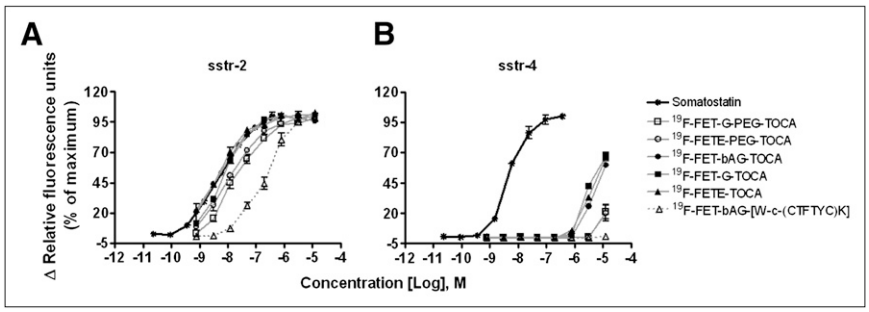

FIGURE 1. Affinity profiles of different ^{18}F-fluoroethyltriazole-Tyr^3-octreotate analogs for sstr subtypes sstr-2 (A) and sstr-4 (B), determined using calcium flux fluorometric imaging plate reader assay as described in "Materials and Methods" section. Assay was performed in duplicate. Fluorescence output was measured and data expressed as percentage maximal fluorescence signal.

ethyltriazole-Tyr^3-octreotate–induced activation of a calcium flux in sstr-2– or sstr-4–expressing Chem-1 cells (Millipore) that were preloaded with a calcium dye. Briefly, Chem-1 cells expressing a specific sstr subtype were seeded in 96-well plates at 50,000 cells per well and incubated in 5% CO_2 for 24 h. Cells were washed and loaded with Fluo-8-No-Wash Ca^{2+} dye in GPCRProfiler Assay Buffer (Millipore) for 90 min at 30°C in a 5% CO_2 incubator. Different concentrations of ^{19}F-fluoroethyltriazole-Tyr^3-octreotate or somatostatin (Sigma; positive control) were added, followed by fluorescence determination. The assay was performed in agonist mode in duplicate. Fluorescence output was measured and data expressed as percentage maximal fluorescence signal after baseline correction. The half maximal receptor activation for the various ligands was estimated by sigmoid dose–response fitting using GraphPad Prism (version 4.00; GraphPad Software) for Windows (Microsoft).

Animals and Tumor Models

Six- to 8-wk-old female BALB/c *nu/nu* athymic mice were obtained from Harlan United Kingdom Ltd. High–sstr-2 pancreatic tumor cell line AR42J (*28*) and low–sstr-2 human colon cancer cell line HCT116 (LGC Standards) were cultured, respectively, in F12K and RPMI 1640 growth medium containing 10% (v/v) fetal bovine serum, 2 mmol/L L-glutamine, 100 units of penicillin per milliliter, and 100 g of streptomycin per milliliter and grown in a 5% CO_2 incubator at 37°C. Tumors were established by subcutaneous injection of 100 μL of phosphate-buffered saline containing 1×10^6 cells. All animal experiments were done by licensed investigators in accordance with the United Kingdom Home Office Guidance on the Operation of the Animal (Scientific Procedures) Act 1986 and within guidelines set out by the United Kingdom National Cancer Research Institute Committee on Welfare of Animals in Cancer Research (*29*). Tumor dimensions were measured continuously using a caliper, and tumor volumes were calculated by volume = $(\pi/6) \times a \times b \times c$, where a, b, and c represent 3 orthogonal axes of the tumor. Mice were used when their tumors reached approximately 200 mm^3.

In Vivo Plasma Stability of ^{18}F-FET-βAG-TOCA

Because ^{18}F-FET-βAG-TOCA was the lead compound in the series, we assessed its in vivo stability. ^{18}F-FET-βAG-TOCA (~3.7 MBq) was injected via the tail vein into non–tumor-bearing BALB/c *nu/nu* mice. Blood was obtained under general isoflurane anesthesia at 30 min after injection, and plasma samples were prepared and immediately frozen on ice. For analysis, the samples were thawed and kept at 4°C immediately before use. Plasma (~0.2 mL) was clarified by addition of ice-cold methanol (1.5 mL), followed by centrifugation of the mixture (3 min, 20,000*g*; 4°C). The supernatant was evaporated to dryness. The residue was resuspended in high-performance liquid chromatography (HPLC) mobile phase (1.2 mL) and clarified (0.2-μm filter), and the sample (1 mL) was injected via a 1-mL sample loop onto the HPLC column. Samples were analyzed by radio-HPLC on a 1100 series HPLC system (Agilent Technologies) equipped with a γ-RAM model 3 γ-detector (IN/US Systems Inc.) and Laura 3 software (Lablogic) and ultraviolet detector (254 nm). A Waters μBondapak C_{18} reversed-phase column (300 × 7.8 mm) stationary phase was eluted with a mobile phase comprising 67% water (0.1% trifluoroacetic acid)/33% acetonitrile (0.1% trifluoroacetic acid) delivered isocratically at 3 mL/min.

PET Studies

Dynamic PET scans were performed on a dedicated small-animal PET scanner (Inveon PET module; Siemens Molecular Imaging Inc.) as reported previously (*29,30*). Briefly, tail veins were cannulated under general anesthesia (isoflurane). The animals were placed within a thermostatically controlled environment within the scanner; heart rate was monitored throughout the study. The mice were injected with 3.0–3.7 MBq of the different radiolabeled compounds, and dynamic PET/CT scans were acquired in list-mode format over 60 min. In the case of ^{18}F-FET-βAG-TOCA, blocking studies were also done, whereby radiotracer injection and imaging commenced 10 min after intravenous injection of 10 mg of unlabeled octreotide per kilogram (Sigma) to mice; this dose of octreotide was approximately 100-fold higher than the equivalent dose of unlabeled ^{18}F-FET-βAG-TOCA in the radiotracer injectate. The acquired data in all cases were sorted into 0.5-mm sinogram bins and 19 time frames ($0.5 \times 0.5 \times 0.5$ mm voxels; 4×15 s, 4×60 s, and 11×300 s) for image reconstruction. Three-dimensional regions of interest were manually defined on 5 adjacent regions: tumor, liver, kidney, muscle, or urine or bladder (each 0.5 mm in thickness). Data were averaged for tissues at each of the 19 time points to obtain time–activity curves. Radiotracer uptake for each tissue was normalized to injected dose and expressed as percentage injected activity per milliliter of tissue (%ID/mL).

Direct Counting of Tissue Radioactivity

After the 60-min PET scan, a part of the tumor tissue was obtained from mice after exsanguination via cardiac puncture under general isoflurane anesthesia. All samples were weighed and their radioactivity directly determined using a Cobra II Auto-gamma-counter (formerly Packard Instruments) applying a decay correction. The results were expressed as a percentage injected dose per gram (%ID/g).

Statistics

Statistical analyses were performed using Prism, version 4.00 (GraphPad). Between-group comparisons were made using the nonparametric Mann–Whitney test. Two-tailed *P* values of 0.05 or less were considered significant.

RESULTS

Radiotracers

All radiotracers were successfully prepared with more than 98% radiochemical purity. The total synthesis time was approximately 1.5 h. Log D of the different tracers is shown in Supplemental Figure 1.

In Vitro sstr Subtype Specificity

All the ^{19}F-fluoroethyltriazole-Tyr^3-octreotate analogs exhibited agonist activity on sstr-2 (Fig. 1; Table 1), with the scrambled peptide (FET-βAG-[W-c-(CTFTYC)K]) having expectedly poor affinity. The affinity of the ligands (half-maximal effective concentration [EC_{50}]) ranged between 4 and 19 nM (vs. somatostatin at 5.6 nM), with the PEG-TOCA analogs showing the lowest affinity to sstr-2. All ^{19}F-fluoroethyltriazole-Tyr^3-octreotate analogs except the scrambled peptide showed detectable activity against sstr-4, but the affinity was poor (≥5.4 mM). None of the compounds exhibited detectable activity against sstr-3 (data not shown).

TABLE 1
sstr-2 and sstr-4 Affinities for Various Agonist ^{19}F-Fluoroethyltriazole-Tyr^3-Octreotate Ligands Expressed as Concentration at Which Half-Maximal Receptor Activation Occurs (Half-Maximal Effective Concentration, EC50)

Compound identity	Predicted agonist EC_{50} potency value	
	sstr-2	sstr-4
Somatostatin	5.6 nM	3.8 nM
^{19}F-FET-G-PEG-TOCA	19.0 nM	>10 mM
^{19}F-FETE-PEG-TOCA	12.0 nM	>10 mM
^{19}F-FET-βAG-TOCA	4.7 nM	8.6 mM
^{19}F-FET-G-TOCA	6.9 nM	5.4 mM
^{19}F-FETE-TOCA	4.1 nM	6.5 mM
^{19}F-FET-βAG-[W-c-(CTFTYC)K]	220 nM	ND

ND = could not be determined because of lack of activity.

^{18}F-FET-βAG-TOCA Stability In Vivo

The in vivo stability of ^{18}F-FET-βAG-TOCA was examined. Typical radiochromatograms of dose solution and 30-min mouse plasma are shown in Figure 2. No metabolites of ^{18}F-FET-βAG-TOCA were seen; only intact parent tracer was found.

Pharmacokinetics and In Vivo Tumor Localization of ^{18}F-Fluoroethyltriazole-Tyr^3-Octreotate Analogs

Given the high affinity and systemic stability of ^{18}F-FET-βAG-TOCA, it was reassuring to observe good localization of the radiotracer in the tumor. Figure 3A shows typical transverse and sagittal PET image slices through sstr-2–expressing AR42J tumor–bearing mice, demonstrating localization of ^{18}F-FET-βAG-TOCA in the tumor, kidney, and bladder or urine, with high signal-to-background contrast. In contrast, no radiotracer localization was seen in tumors of the mice when the scrambled peptide ^{18}F-FET-βAG-[W-c-(CTFTYC)K] was injected (Fig. 3B). In this case, tracer localization was seen mainly in the brain, urine, liver, and intestines (data not shown). The comparative pharmacokinetics of all ^{18}F-fluoroethyltriazole-Tyr^3-octreotate analogs in the tumor, kidney, liver, and muscle are shown in Figure 4; liver tissue data with expanded *y*-axis and bladder or urine data are shown in Supplemental Figure 2. Radiotracer uptake in the AR42J tumor was characterized by a rapid increase over the entire scanning period of 60 min. ^{18}F-FET-G-TOCA had the highest tumor uptake, followed by ^{18}F-FET-βAG-TOCA, which had uptake higher than or comparable to ^{18}F-AIF-NOTA-OC. These tracers were superior to the clinical radiotracer ^{68}Ga-DOTATATE with respect to tumor uptake as well as tumor-to-muscle and tumor-to-blood ratios (Table 2). Because the animals were scanned on different days, the mean specific radioactivity for each radiotracer is presented (Table 2). PEG linkers, embodied within the structures of ^{18}F-FET-G-PEG-TOCA and ^{18}F-FETE-PEG-TOCA, reduced tumor uptake but increased tumor-to-muscle and tumor-to-blood ratios (Fig. 4; Table 2). Nonspecific uptake in liver was, in general, low (<7 %ID/mL), with ^{18}F-FET-βAG-TOCA showing the lowest liver uptake; ^{18}F-FET-G-TOCA and ^{18}F-FETE-PEG-TOCA showed the highest liver uptake. The ^{18}F PEG-TOCA analogs had the highest urinary clearance, in keeping with their lower lipophilicity. Radiotracer kinetic profiles in the kidney, which also expresses sstr-2 (*31*), were different from those in tumors; however, the magnitude of uptake was highest for the 2 radiotracers ^{18}F-FET-βAG-TOCA and ^{18}F-FET-G-TOCA. The mean muscle uptake was less than 3 %ID/mL for all radiotracers. Radiotracer uptake in the bone was low for all the analogs, indicating little or no defluorination. We compared the uptake of the radiotracers in the imaging studies to direct tissue counting. The profiles were generally in agreement, but the magnitude was higher for direct counting, consistent with partial-volume averaging. Direct radioactivity determination (γ-counting) of only a part of the tissue relative to sampling of the whole tumor in the case of imaging could also have led to systematic differences.

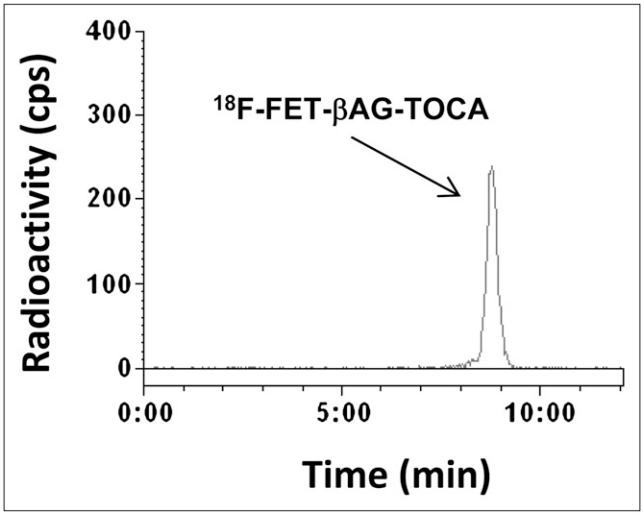

FIGURE 2. Radio-HPLC of ^{18}F-FET-βAG-TOCA. Typical plasma extract obtained 30 min after injection of radiotracer into mice, indicating metabolically stable radiotracer. Dose solution was used as reference standard and also showed analyte retention at 8.47 min. cps = counts per second.

Specificity of ^{18}F-FET-βAG-TOCA Uptake

Given the high tumor uptake of the radiotracers, we next assessed the specificity of uptake in vivo using ^{18}F-FET-βAG-TOCA as the prototypical ^{18}F-fluoroethyltriazole-Tyr^3-octreotate. We demonstrated that radiotracer uptake was specific: in keeping with the poor affinity for sstr-2, the radiolabeled scrambled peptide ^{18}F-FET-βAG-[W-c-(CTFTYC)K] did not show detectable tumor uptake in the AR42J model in vivo (Fig. 5). ^{18}F-FET-βAG-[W-c-(CTFTYC)K] uptake was higher in liver than ^{18}F-FET-βAG-TOCA. To show that the tumor uptake of radiotracer

RGB

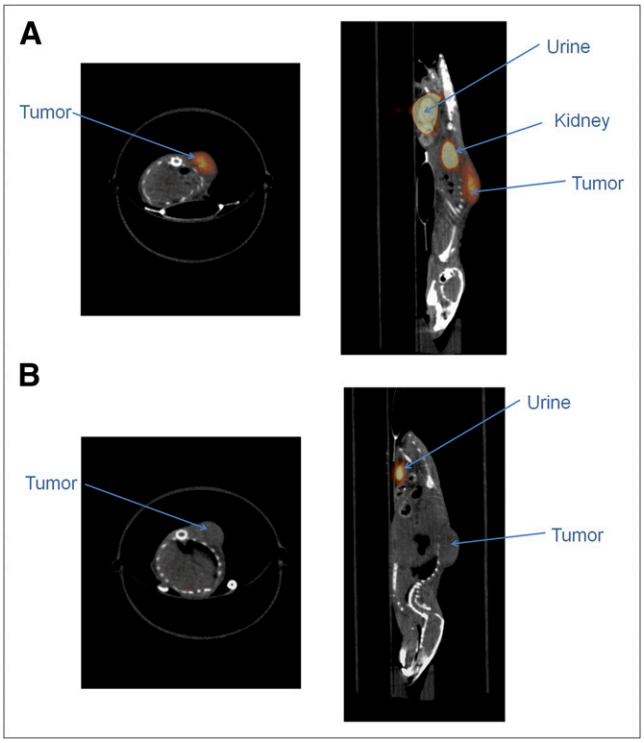

FIGURE 3. PET/CT images showing localization of ^{18}F-FET-βAG-TOCA (A) and scrambled peptide ^{18}F-FET-βAG-[W-c-(CTFTYC)K] (B) in tumors, kidney, and bladder (urine) of AR42J tumor–bearing mice. Transverse and sagittal static (30–60 min, fused; 0.5-mm slice) images are presented.

was receptor-mediated, blocking studies were conducted by preinjecting mice with an excess of unlabeled octreotide (100-fold molar equivalent) to saturate sstr-binding sites. This resulted in a 2-fold (by direct counting) lower uptake of ^{18}F-FET-βAG-TOCA in AR42J xenografts and even higher reductions in tumor-to-muscle and tumor-to-blood ratios (Fig. 5; Table 2). After blocking with unlabeled octreotide, muscle radioactivity increased. Kidney (early time points only) decreased but subsequently increased; urine radioactivity decreased (Supplemental Fig. 3). Further evidence for the specificity of ^{18}F-FET-βAG-TOCA uptake was provided by the low uptake in low–sstr-expressing HCT116 xenografts, compared with the AR42J xenografts (Table 2).

DISCUSSION

We report here new ^{18}F-fluoroethyltriazole-Tyr^3-octreotate radioligands that combine high specific binding with rapid target localization for high-contrast PET. Six ^{18}F-fluoroethyltriazole-Tyr^3-octreotate analogs were synthesized by the click reaction, and their in vitro affinity and in vivo pharmacokinetics were investigated to enable selection of the optimal radiotracer for PET of somatostatin receptor–positive GEP-NETs. The current somatostatin receptor–based clinical standard for functional imaging, ^{111}In-DTPA-octreotide, suffers from low image contrast and uses a long (1–2 d) diagnostic protocol (*9*). Substitution of Phe^3 by Tyr^3 on octreotide, as well as C-terminal Thr(ol)^8 by Thr, gives Tyr^3-octreotate [(D)-Phe^1-c(Cys^2-Tyr^3-(D)-Trp^4-Lys^5-Thr^6-Cys^7)Thr^8], with improved selectivity and affinity for sstr-2 (*8,11,12*). We have now further modified Tyr^3-octreotate by introducing an ^{18}F-labeled triazole via the click reaction (*24*). For these ^{18}F-labeled compounds to be useful, however, they need to combine high tumor uptake with rapid low nontarget washout. We used different chain lengths,

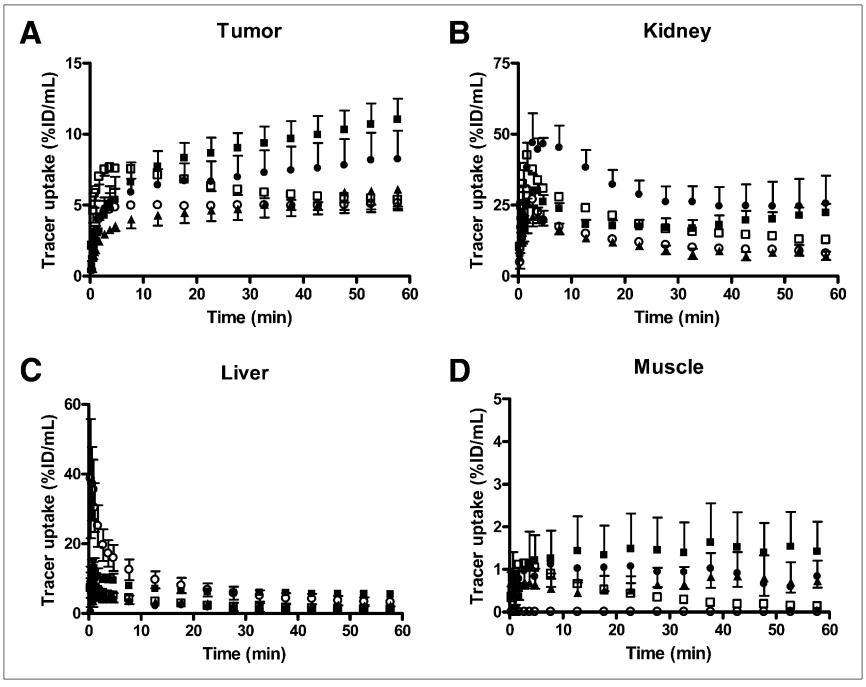

FIGURE 4. Time–activity curves comparing tissue pharmacokinetics of ^{18}F-fluoroethyltriazole-Tyr^3-octreotate analogs in AR42J tumor (A), kidney (B), liver (C), and muscle (D). Dynamic PET/CT was performed for 60 min after intravenous injection of each radiotracer into tumor-bearing mice. Tissue radiotracer uptake values are expressed as %ID/mL of tissue. Values represent mean ± SEM (n = 3–5); for clarity, only upper or lower error bars are plotted. □ = ^{18}F-FET-G-PEG-TOCA; ○ = ^{18}F-FETE-PEG-TOCA; ● = ^{18}F-FET-βAG-TOCA; ■ = ^{18}F-FET-G-TOCA; ▲ = ^{18}F-FETE-TOCA.

TABLE 2
Comparison of Tissue Uptake of ^{18}F-Octreotate Analogs in AR42J and HCT116 Tumor Xenografts

Octreotate analog	Specific radioactivity (GBq/μmol)*	Tumor studied	Tumor tracer uptake... At 60 min by imaging (%ID/mL)	Tumor tracer uptake... After 60 min by γ-counting (%ID/g)	Muscle tracer uptake after 60 min by γ-counting (%ID/g)	Blood tracer uptake after 60 min by γ-counting (%ID/g)	Mean... Tumor-to-muscle ratio (60 min)	Mean... Tumor-to-blood ratio (60 min)
^{18}F-FET-G-PEG-TOCA	4.8	AR42J	5.36 ± 0.45	8.29 ± 1.42	0.14 ± 0.10	0.35 ± 0.22	59.21	23.69
^{18}F-FETE-PEG-TOCA	5.9	AR42J	5.14 ± 0.40	4.51 ± 1.52	0.19 ± 0.05	0.21 ± 0.03	23.74	21.48
^{18}F-FET-G-TOCA	5.9	AR42J	11.00 ± 1.49	17.05 ± 2.77	1.49 ± 0.59	1.61 ± 0.65	11.44	10.59
^{18}F-FETE-TOCA	8.4	AR42J	6.11 ± 1.46	9.79 ± 2.57	0.79 ± 0.23	1.05 ± 0.32	12.39	9.32
^{18}F-FET-βAG-TOCA	3.9	AR42J	8.23 ± 2.02	11.58 ± 0.67	0.48 ± 0.21	0.86 ± 0.27	24.12	13.47
^{18}F-FET-βAG-TOCA	18.7	HCT116	2.42 ± 0.35	0.52 ± 0.39	0.58 ± 0.45	1.19 ± 0.89	0.97	0.44
^{18}F-FET-βAG-TOCA blocking	11.2	AR42J	6.24 ± 0.64	3.93 ± 0.99	1.39 ± 0.51	0.63 ± 0.54	2.83	6.24
^{18}F-FET-βAG-[W-c-(CTFTYC)K	12.3	AR42J	0.10 ± 0.05	0.22 ± 0.12	0.34 ± 0.30	0.20 ± 0.01	0.65	1.10
^{18}F-AIF-NOTA-OC	36.1	AR42J	6.43 ± 0.85	12.73 ± 2.05	0.34 ± 0.10	0.55 ± 0.24	37.44	23.15
^{68}Ga-DOTATATE	ND	AR42J	2.75 ± 0.11	1.37 ± 0.16	0.60 ± 0.08	2.45 ± 0.56	2.28	0.56

*Determined at end of synthesis.
ND = Not determined.
Data are mean ± SE, n = 3–6. Imaging data are presented for 60-min time point together with tissue data obtained from counting pieces of tissue directly in γ-counter soon after imaging study. In vivo ^{18}F-FET-βAG-TOCA blocking studies were done after intravenous injection of unlabeled octreotide (10 mg/kg) to mice, followed 10 min later by injection of radiotracer.

alkyl groups, or PEG groups to enable evaluation of the impact of physicochemical variables on pharmacokinetics.

In vitro studies revealed that the triazole analogs had high selective affinity to sstr-2, with half-maximal agonist activity in the calcium flux assay for this G-protein–coupled receptor (EC_{50}) ranging from 4 to 19 nM, compared with the scrambled peptide, which had a low affinity. The combined effect of high binding affinity for sstr and rapid washout from nontarget tissue produced high-contrast PET images in vivo, demonstrated for ^{18}F-FET-βAG-TOCA in Figure 3. The increasing tumor time versus activity curves of ^{18}F-FET-βAG-TOCA derived from the in vivo dynamic PET image data (Fig. 4) reflected the high selective binding of ^{18}F-FET-βAG-TOCA. The radiotracer was metabolically stable in mice and was not defluorinated. Overall, we observed that ^{18}F-fluoroethyltriazole-Tyr^3-octreotate radiotracer pharmacokinetics was modified by the structural changes. For example, ^{18}F-FET-G-TOCA that differed in 1 amino acid group (β-alanine) from ^{18}F-FET-βAG-TOCA showed higher tumor uptake and higher nonspecific tissue uptake. This observation may be because of the higher lipophilicity of FET-G-TOCA. Use of ethylene (^{18}F-FET-G-TOCA) instead of amide linker (^{18}F-FETE-TOCA) led to differences in tumor uptake, despite similar sstr-2 agonist affinities in vitro. Thus, chain length and linker type affects pharmacokinetics, but we did not have enough

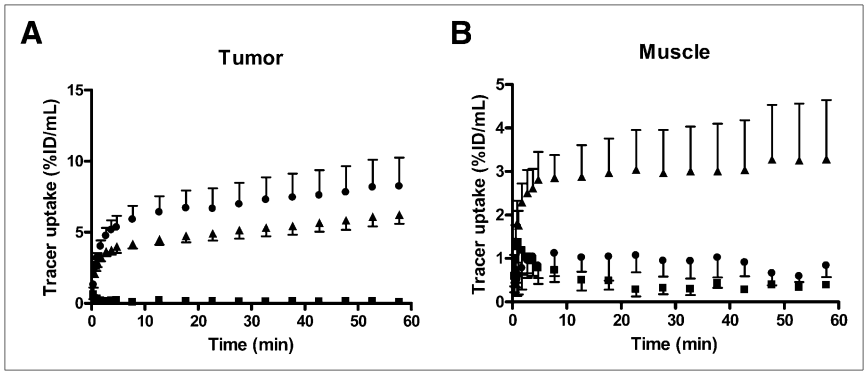

FIGURE 5. Specificity of ^{18}F-FET-βAG-TOCA localization in AR42J xenograft model. Kinetics of ^{18}F-FET-βAG-TOCA are shown, along with effect of saturating receptor binding sites with excess cold unlabeled octreotide in tumor (A) and muscle (B). Blocking studies were performed by injecting octreotide (10 mg/kg; intravenously) 10 min before intravenous injection of ^{18}F-FET-βAG-TOCA. Dynamic imaging was performed over 60 min. Tissue radiotracer uptake values are expressed as %ID/mL of tissue. The graphs also illustrate pharmacokinetics of scrambled peptide ^{18}F-FET-βAG-[W-c-(CTFTYC)K] in same mouse model. Values represent mean ± SEM (n = 3–5); for clarity, only upper or lower error bars are plotted. ● = ^{18}F-FET-βAG-TOCA in octreotide-naïve mice; ▲ = ^{18}F-FET-βAG-TOCA in mice predosed with 10 mg of unlabeled octreotide per kilogram; ■ = ^{18}F-FET-βAG-[W-c-(CTFTYC)K in octreotide-naïve mice.

analog data to predict the mechanisms underpinning this effect.

Interestingly, the tumor uptake for ^{18}F-FET-G-TOCA and ^{18}F-FET-βAG-TOCA compounds ranked among the highest reported to date and was higher than that of ^{68}Ga-DOTATATE (Table 1), which is used clinically. Similarly the tumor uptake of the two ^{18}F-fluoroethyltriazole-Tyr^3-octreotate analogs was significantly higher than those reported for ^{111}In-DTPA-octreotide by Froidevaux et al. in the same tumor model (3.03 ± 0.26 %ID/g) (*32*). The tracers also showed uptake similar to or higher than ^{18}F-AIF-NOTA-OC. In contrast to the high tumor uptake of ^{18}F-FET-G-TOCA and ^{18}F-FET-βAG-TOCA, the 2 PEGylated analogs showed lower tumor uptake. Because of reduced glomerular filtration, PEGylation of peptides reduces their overall clearance from the body and increases half-life. We used only small PEG groups of approximately 0.3 kDa, which may not be large enough to affect glomerular filtration. PEGylation also makes compounds more water-soluble (*33*), supporting faster clearance from the circulation than with the less hydrophilic non-PEGylated analogs. The high urinary clearance of our PEGylated analogs (Supplemental Fig. 2) and high tumor-to-muscle and tumor-to-blood ratios supported the latter mechanism. The low overall tumor uptake of the PEG-TOCA analogs could also be explained by their lower in vitro affinity (Fig. 1; Table 1).

It was predicted that liver tissue that generally shows low ^{111}In-DTPA-octreotide uptake (*34*) will also show low uptake of the ^{18}F-fluoroethyltriazole-Tyr^3-octreotate radiotracers. The PEG-TOCA analogs had lower liver uptake. Interestingly, ^{18}F-FET-βAG-TOCA, with intermediate hydrophilicity, compared with the PEGylated analogs (Supplemental Fig. 1), showed similar low uptake in liver, a positive attribute of ^{18}F-FET-βAG-TOCA that was not realized in ^{18}F-FET-G-TOCA. High nonspecific liver uptake could reduce specificity of imaging agents for detecting metastatic liver disease. ^{18}F-FET-G-TOCA had high liver uptake, making it less attractive for imaging metastatic disease despite showing the highest tumor uptake. Because of its high specificity, characterized by high tumor uptake and tumor-to-muscle ratio but comparatively low background (liver) uptake, we selected ^{18}F-FET-βAG-TOCA for further evaluation.

Evidence from the blocking studies and poor uptake in low-sstr tumors with respect to ^{18}F-FET-βAG-TOCA, as well as low tumor uptake of the scrambled peptide, indicated that the uptake of ^{18}F-FET-βAG-TOCA was receptor-mediated. The in vivo blocking study showed that injecting unlabeled octreotide partially reduced tumor uptake of ^{18}F-FET-βAG-TOCA in the AR42J model. Muscle and liver retained higher radioactivity levels with blocking, possibly because of reduced elimination into urine. Interestingly, the kidney uptake normalized at late time points after blocking. The kidney is a complex organ regarding uptake of somatostatin analogs. The kidney profile observed in our dynamic study may be due to a mix of receptor-mediated and non–receptor-mediated effects (*35*). For radiometal-labeled octreotide analogs, non–receptor-mediated mechanisms appear to dominate uptake (*36*). The mechanism for the non–receptor-mediated renal uptake is generally assumed to involve charge-dependent endocytosis in kidneys; in keeping with this assumption, coinfusion of basic amino acids selectively reduces accumulation in kidneys (*20,37,38*). Other radiometal-labeled peptides including bombesin also show high kidney uptake; however, kidney uptake of labeled peptides is modified by the radioactive label used. Indeed, work by Liu et al. showed that for radiolabeled bombasin, renal uptake decreases in the order ^{64}Cu > ^{68}Ga >> ^{18}F. Therefore, for ^{18}F-octreotate analogs, specific uptake by renal sstr-2 may contribute significantly to uptake, explaining the initial reduction of uptake in kidneys after injection of excess unlabeled octreotide. We also interpret the low renal uptake of the scrambled peptide that had poor in vitro affinity for sstr-2 as resulting at least in part from low receptor binding. Excess cold octreotide may affect renal solute transport. High-dose somatostatin decreases renal plasma flow and glomerular filtration rate in humans (*39*); the same effect would be expected of other agonists in the mouse given expression of sstr-2 in mouse kidney (*31*) and could explain the lower urine levels after treatment with cold octreotide. Similarly, we speculate that the smaller than expected reduction in kidney radiotracer uptake at late time points after administration of excess cold ligand could be due in part to reduced renal plasma flow and glomerular filtration. Finally, uptake in AR42J was higher than that in HCT116, in keeping with the higher receptor expression in the former (sstr maximal receptor binding [Bmax], 2,482 fmol of protein per milligram for AR42J vs. 678 fmol of protein per milligram for HCT116 (*28,40*)). These studies demonstrate specificity of the radiotracers for imaging sstr-2–expressing tumors.

CONCLUSION

We report for the first time, to our knowledge, ^{18}F-fluoroethyl-triazole-Tyr^3-octreotate radioligands developed via click chemistry that have good stability, high binding affinity, and optimal pharmacokinetics for imaging sstr-2–positive tumors at early time points. The prerequisite for use of short-lived positron-emitting radioisotopes involving rapid tumor accumulation together with rapid clearance of labeled peptides from normal non–sstr-expressing tissues was met but not through use of the PEG moiety. This unique multiradiotracer design and in vivo assessment has enabled us to select 2 radiotracers, ^{18}F-FET-βAG-TOCA and ^{18}F-FET-G-TOCA, as candidate sstr-2 imaging agents for clinical examination.

DISCLOSURE STATEMENT

The costs of publication of this article were defrayed in part by the payment of page charges. Therefore, and solely to indicate this fact, this article is hereby marked "advertisement" in accordance with 18 USC section 1734.

ACKNOWLEDGMENT

We thank Dr. Graham Smith for supporting metabolism studies of ^{18}F-FET-βAG-TOCA. We acknowledge funding support from a U.K. Medical Research Council Developmental Pathway Funding Scheme project grant (G0801762) and Cancer Research U.K.–Engineering and Physical Sciences Research Council Centre grant (C2536/A10337). We thank the staff at the Biological Imaging Centre at Imperial College for their support. The authors have filed a patent on this invention. No other potential conflict of interest relevant to this article was reported.

REFERENCES

1. Modlin IM, Oberg K, Chung DC, et al. Gastroenteropancreatic neuroendocrine tumors. *Lancet Oncol.* 2008;9:61–72.
2. Rinke A, Muller HH, Schade-Brittinger C, et al. Placebo-controlled, double-blind, prospective, randomized study on the effect of octreotide LAR in the control of tumor growth in patients with metastatic neuroendocrine midgut tumors: a report from the PROMID Study Group. *J Clin Oncol.* 2009;27:4656–4663.
3. Kulke MH, Siu LL, Tepper JE, et al. Future directions in the treatment of neuroendocrine tumors: consensus report of the National Cancer Institute Neuroendocrine Tumor clinical trials planning meeting. *J Clin Oncol.* 2011;29:934–943.
4. Yao JC, Shah MH, Ito T, et al. Everolimus for advanced pancreatic neuroendocrine tumors. *N Engl J Med.* 2011;364:514–523.
5. Patel YC. Somatostatin and its receptor family. *Front Neuroendocrinol.* 1999;20:157–198.
6. Garcea G, Ong SL, Maddern GJ. The current role of PET-CT in the characterization of hepatobiliary malignancies. *HPB (Oxford).* 2009;11:4–17.
7. Reubi JC. Neuropeptide receptors in health and disease: the molecular basis for in vivo imaging. *J Nucl Med.* 1995;36:1825–1835.
8. Reubi JC, Schar JC, Waser B, et al. Affinity profiles for human somatostatin receptor subtypes SST1-SST5 of somatostatin radiotracers selected for scintigraphic and radiotherapeutic use. *Eur J Nucl Med.* 2000;27:273–282.
9. Krenning EP, Kwekkeboom DJ, Bakker WH, et al. Somatostatin receptor scintigraphy with [^{111}In-DTPA-D-Phe1]- and [^{123}I-Tyr3]-octreotide: the Rotterdam experience with more than 1000 patients. *Eur J Nucl Med.* 1993;20:716–731.
10. Rufini V, Calcagni ML, Baum RP. Imaging of neuroendocrine tumors. *Semin Nucl Med.* 2006;36:228–247.
11. de Jong M, Breeman WA, Bakker WH, et al. Comparison of ^{111}In-labeled somatostatin analogues for tumor scintigraphy and radionuclide therapy. *Cancer Res.* 1998;58:437–441.
12. Schottelius M, Reubi JC, Eltschinger V, Schwaiger M, Wester HJ. N-terminal sugar conjugation and C-terminal Thr-for-Thr(ol) exchange in radioiodinated Tyr3-octreotide: effect on cellular ligand trafficking in vitro and tumor accumulation in vivo. *J Med Chem.* 2005;48:2778–2789.
13. Anderson CJ, Pajeau TS, Edwards WB, Sherman EL, Rogers BE, Welch MJ. In vitro and in vivo evaluation of copper-64-octreotide conjugates. *J Nucl Med.* 1995;36:2315–2325.
14. Jamar F, Barone R, Mathieu I, et al. 86Y-DOTA0)-D-Phe1-Tyr3-octreotide (SMT487)–a phase 1 clinical study: pharmacokinetics, biodistribution and renal protective effect of different regimens of amino acid co-infusion. *Eur J Nucl Med Mol Imaging.* 2003;30:510–518.
15. Kowalski J, Henze M, Schuhmacher J, Macke HR, Hofmann M, Haberkorn U. Evaluation of positron emission tomography imaging using [^{68}Ga]-DOTA-D Phe (1)-Tyr(3)-Octreotide in comparison to [^{111}In]-DTPAOC SPECT: first results in patients with neuroendocrine tumors. *Mol Imaging Biol.* 2003;5:42–48.
16. Miederer M, Seidl S, Buck A, et al. Correlation of immunohistopathological expression of somatostatin receptor 2 with standardised uptake values in ^{68}Ga-DOTATOC PET/CT. *Eur J Nucl Med Mol Imaging.* 2009;36:48–52.
17. Hanaoka H, Tominaga H, Yamada K, et al. Evaluation of ^{64}Cu-labeled DOTA-D-Phe(1)-Tyr (3)-octreotide (^{64}Cu-DOTA-TOC) for imaging somatostatin receptor-expressing tumors. *Ann Nucl Med.* 2009;23:559–567.
18. Guhlke S, Wester HJ, Bruns C, Stocklin G. (2-[^{18}F]fluoropropionyl-(D)phe1)-octreotide, a potential radiopharmaceutical for quantitative somatostatin receptor imaging with PET: synthesis, radiolabeling, in vitro validation and biodistribution in mice. *Nucl Med Biol.* 1994;21:819–825.
19. Laverman P, McBride WJ, Sharkey RM, et al. A novel facile method of labeling octreotide with ^{18}F-fluorine. *J Nucl Med.* 2010;51:454–461.
20. Schottelius M, Poethko T, Herz M, et al. First ^{18}F-labeled tracer suitable for routine clinical imaging of sst receptor-expressing tumors using positron emission tomography. *Clin Cancer Res.* 2004;10:3593–3606.
21. Kayani I, Bomanji JB, Groves A, et al. Functional imaging of neuroendocrine tumors with combined PET/CT using ^{68}Ga-DOTATATE (DOTA-DPhe1,Tyr3-octreotate) and ^{18}F-FDG. *Cancer.* 2008;112:2447–2455.
22. Meisetschlager G, Poethko T, Stahl A, et al. Gluc-Lys([^{18}F]FP)-TOCA PET in patients with SSTR-positive tumors: biodistribution and diagnostic evaluation compared with [^{111}In]DTPA-octreotide. *J Nucl Med.* 2006;47:566–573.
23. Marik J, Sutcliffe JL. Click for PET: rapid preparation of [F-18]fluoropeptides using Cu-I catalyzed 1,3-dipolar cycloaddition. *Tetrahedron Lett.* 2006;47:6681–6684.
24. Glaser M, Årstad E. "Click labeling" with 2-[18f]fluoroethylazide for positron emission tomography. *Bioconjug Chem.* 2007;18:989–993.
25. Glaser M, Robins E. 'Click labeling' in PET radiochemistry. *J Labelled Comp Radiopharm.* 2009;52:407–414.
26. Ramenda T, Kniess T, Bergmann R, Steinbach J, Wuest F. Radiolabeling of proteins with fluorine-18 via click chemistry. *Chem Commun (Camb).* 2009;7521–7523.
27. Iddon L, Leyton J, Indrevoll B, et al. Synthesis and in vitro evaluation of [^{18}F] fluoroethyl triazole labelled [Tyr3]octreotate analogues using click chemistry. *Bioorg Med Chem Lett.* 2011;21:3122–3127.
28. Taylor JE, Theveniau MA, Bashirzadeh R, Reisine T, Eden PA. Detection of somatostatin receptor subtype 2 (SSTR2) in established tumors and tumor cell lines: evidence for SSTR2 heterogeneity. *Peptides.* 1994;15:1229–1236.
29. Workman P, Aboagye EO, Balkwill F, et al. Guidelines for the welfare and use of animals in cancer research. *Br J Cancer.* 2010;102:1555–1577.
30. Leyton J, Alao JP, Da Costa M, et al. In vivo biological activity of the histone deacetylase inhibitor LAQ824 is detectable with 3′-deoxy-3′-[^{18}F]fluorothymidine positron emission tomography. *Cancer Res.* 2006;66:7621–7629.
31. Bates CM, Kegg H, Grady S. Expression of somatostatin receptors 1 and 2 in the adult mouse kidney. *Regul Pept.* 2004;119:11–20.
32. Froidevaux S, Heppeler A, Eberle AN, et al. Preclinical comparison in AR4-2J tumor-bearing mice of four radiolabeled 1,4,7,10-tetraazacyclododecane-1,4,7,10-tetraacetic acid-somatostatin analogs for tumor diagnosis and internal radiotherapy. *Endocrinology.* 2000;141:3304–3312.
33. Veronese FM, Mero A. The impact of PEGylation on biological therapies. *BioDrugs.* 2008;22:315–329.
34. Hofland LJ, Lamberts SW, van Hagen PM, et al. Crucial role for somatostatin receptor subtype 2 in determining the uptake of [^{111}In-DTPA-D-Phe1]octreotide in somatostatin receptor-positive organs. *J Nucl Med.* 2003;44:1315–1321.
35. Melis M, Krenning EP, Bernard BF, Barone R, Visser TJ, de Jong M. Localisation and mechanism of renal retention of radiolabeled somatostatin analogues. *Eur J Nucl Med Mol Imaging.* 2005;32:1136–1143.
36. de Jong MW, Pinas IM, van Eijck J. Delayed interval delivery after intrauterine infection and immature birth of twin 1: a case report and literature review. *Eur J Obstet Gynecol Reprod Biol.* 1995;63:91–94.
37. Akizawa H, Arano Y, Mifune M, et al. Effect of molecular charges on renal uptake of ^{111}In-DTPA-conjugated peptides. *Nucl Med Biol.* 2001;28:761–768.
38. Behr TM, Goldenberg DM, Becker W. Reducing the renal uptake of radiolabeled antibody fragments and peptides for diagnosis and therapy: present status, future prospects and limitations. *Eur J Nucl Med.* 1998;25:201–212.
39. Vora JP, Owens DR, Ryder R, Atiea J, Luzio S, Hayes TM. Effect of somatostatin on renal function. *Br Med J (Clin Res Ed).* 1986;292:1701–1702.
40. Szepeshazi K, Schally AV, Halmos G, et al. Targeted cytotoxic somatostatin analogue AN-238 inhibits somatostatin receptor-positive experimental colon cancers independently of their p53 status. *Cancer Res.* 2002;62:781–788.